Analytical Methods

Accepted Manuscript

This article can be cited before page numbers have been issued, to do this please use: X. Yao, J. Shen, Q. Liu, H. Fa, M. Yang and C. Hou, *Anal. Methods*, 2020, DOI: 10.1039/D0AY01503B.

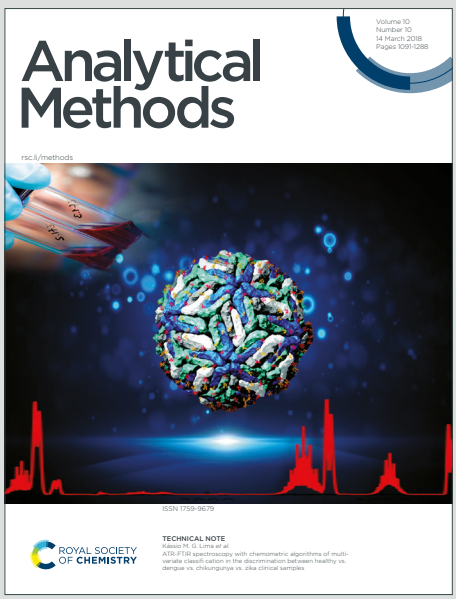

ROYAL SOCIETY OF CHEMISTRY

rsc.li/methods

A novel electrochemical aptasensor for sensitive detection of kanamycin based on UiO-66-NH_2/MCA/MWCNT@rGONR nanocomposite

Xin Yao,[a,b] Jinhui Shen,[a,b] Qingyan Liu,[a,b] Huanbao Fa,[c] Mei Yang,[a,b,*] Changjun Hou[a,b,*]

[a] Key Laboratory of Biorheological Science and Technology, Ministry of Education, College of Bioengineering, Chongqing University, Chongqing 400044, PR China

[b] College of Bioengineering, Chongqing University, Chongqing 400044, PR China

[c] College of Chemistry and Chemical Engineering, Chongqing University, Chongqing 400044, PR China

[*] Corresponding authors.

E-mail addresses: yangmei@cqu.edu.cn (M. Yang); houcj@cqu.edu.cn (C.J. Hou)

Tel: +86 23 6511 2673; Fax: +86 23 6510 2507

Abstract: In this work, we designed and synthesized a nanocomposite of amine-functionalized metal organic framework (UiO-66-NH_2), multiwalled carbon nanotube@reduced graphene oxide nanoribbon (MWCNT@rGONR) and a covalent organic framework (COF) synthesized by melamine and cyanutic acidmonomers through polycondensation (represented by MCA). The UiO-66-NH_2/MCA/MWCNT@rGONR nanocomposite was used as a sensitive platform for an electrochemical aptasensor to detect kanamycin (kana). Owning to the rich chemical functionality, amino-rich structure and excellent electrochemical activity, the cDNA strands terminated by amino, can not only anchor over the UiO-66-NH_2/MCA/MWCNT@rGONR surface but also can penetrate into the interior of porous UiO-66-NH_2/MCA/MWCNT@rGONR networks. The characterization of UiO-66-NH_2/MCA/MWCNT@rGONR nanocomposite was performed by scanning electronic microscopy (SEM), X-ray photoelectron spectroscopy (XPS), fourier transform infrared spectroscopy (FT-IR) and X-ray diffraction (XRD). Furthermore, cyclic voltammetry (CV) and square wave voltammetry (SWV) were employed for the electrochemical performance study of this biosensor. According to the results, UiO-66-NH_2/MCA/ MWCNT@rGONR nanocomposite exhibited high bioaffinity toward the aptamer, and the lowest limit of detection at 13 nM (S/N = 3) within a linearity of the kana concentration of 25~900 nM. In addition, it possessed great repeatability, stability and selectivity and obtained satisfactory recovery results in real analysis of fish meat and milk, indicating the great potential for analytical measurements in food safety.

Key words: kanamycin; UiO-66-NH_2; MWCNT@rGONR; MCA; electrochemical aptasensor

View Article Online
DOI: 10.1039/D0AY01503B

1. Introduction

Antibiotics are antibacterial drugs that can be used as growth promoters in animals and for treating infections [1, 2]. Kanamycin is a bactericidal antibiotic isolated from Streptomyces kanamyceticus [3], whose spectrum of activity comprises Gram-negative and Gram-positive bacteria [4, 5]. Widely used as veterinary medicine to treat serious animal diseases [6], such as urinary septicemia, pneumonia, and intestinal infections [7]. However, all the antibiotic drugs are not safe for the treatment of bacterial infection of animals as some of them are threating human beings health. The food safety has always been an important issue and a universal concern. Because human are at the top of the food chain, and the biological enrichment effect of antibiotics will cause great harm to humans. Thus if we uncontrolled use of kana, it may not only cause serious threats to human health [3, 8], such as hypersensitivity, drug resistance and toxicity, but may also cause disturbed environmental flora [9]. The United States mandates that no antibiotic residues should be detected in milk. The European Union also strictly regulates the maximum residue (MRL) of antibiotics: the aminoglycoside antibiotic Kanamycin (150 ng / ml) in milk. Therefore, there is an urgent need to develop a sensitive, efficient and fast determination method to detect antibiotic residues in foods.

Currently, various methods have been reported to achieve efficient detection of antibiotic residues in food, such as high performance liquid chromatography (HPLC) [10, 11], high performance liquid chromatography-tandem mass spectrometry (HPLC-MS/MS) [12], fluorescence polarization immunization (FPIA) [13], colorimetric (CO) [14-16], enzyme-linked immunosorbent assay (ELISA) [17], electrochemiluminescent [18, 19], fluorescent (FL) [19], Fluoroimmunoassay (FIA) [20, 21] and photoelectrochemical (PEC) [22]. Electrochemistry, as one

View Article Online
DOI: 10.1039/D0AY01503B

of the most commonly used technologies for antibiotic residues detection [8]. Compared to optical sensors, electrochemical sensors are more sensitive and have attained a great deal of attention in the detection of antibiotics [23-25].

On the other hand, aptamers, with the advantage of high selectivity and high specificity to targets and easy to be synthetic in vitro, have provided a broad prospect for developing electrochemical sensing system [26]. Electrochemical sensors combined with aptamer technology will significantly improve selectivity and sensitivity, aptamer technology has great application prospects in antibiotic detection [27-29]. For example, a label-free electrochemical biosensor detection of kana based on polymer-Au nanocomposite and aptamer modified disposable screen-printed electrode was reported by Zhu et al [30], and the biosensor with the lowest limit of detection at 9.4±0.4 nM within a linear range of 0.05 μM to 9.0 μM. Zhou et al [31] synthesized a series of nanohybrids of the covalent organic framework (COF) and Ce-based metal organic framework (MOF) as bioplatforms to detect oxytetracycline and exhibited the lowest limit of detection at 17.4 fM within a linear range of 0.1-0.5 nM. Zhu et al [32] reported a new electrochemical biocode based on MOF, which was developed to detect multiple antibiotics simultaneously, such as kanamycin and chloramphenicol with detection limits as 0.16 pM and 0.19 pM (S/N=3) toward respectively. Due to the various grafting groups and excellent adsorption characteristics (e.g. NH_2 or COOH), the porous COFs and MOFs are ideal choices, which may facilitate the co-immobilization of biological ligands like aptamer [33, 34]. It is worth mentioning that nanoscale MOFs and COFs with large dispersion and specific surface area, are suitable for the assembly of biological codes.

However, previous electrochemical biosensors combined with aptamer have poor

View Article Online
DOI: 10.1039/D0AY01503B

stability and repeatability because the fixation effect of the aptamer on the base material was unstable. Furthermore, labelling the aptamer with an electrical signal group will affect its binding affinity to the target, and this kind of biomaterial which loaded on the electrode will heavily decrease the electrochemical signal and have a great influence on the performance of the sensor. In order to carry out more effective antibiotic detection, we need to develop a more stable and reproducible electrochemical biosensor. We can improve the incubation effect of the aptamer and the strength of the electrochemical signal by choosing a more powerful material to modify the electrode.

In this work, we synthesized a novel kind of UiO-66-NH_2/MCA/MWCNT@rGONR nanohybrid with MOF (UiO-66-NH_2), COF (synthesized by melamine and cyanutic acidmonomers, represented by MCA) and multiwalled carbon nanotube@reduced graphene oxide nanoribbon (MWCNT@rGONR), and used the nanohybrid to detect kanamycin electrochemically for the first time. In the nanohybrid, UiO-NH_2-66 and MCA facilitated the covalent immobilization of aptamer owing to the presence of more active sites and abundant amino group on their surface. Due to the rich chemical functionality, amino-rich structure and excellent electrochemical activity, the aptamer's complementary DNA (cDNA) strands terminated by amino could not only anchor over the UiO-66-NH_2/MCA surface but also could penetrate into the interior of porous UiO-66-NH_2/MCA networks by π-π stacking interaction and electrostatic interaction between the organic frameworks and the cDNA strands. In addition, the carbon substances MWCNT@rGONR, with a core-shell heterostructure, possessed the large surface area and high electronic conductivity. Definitively, the as-prepared UiO-66-NH_2/MCA/MWCNT@rGONR nanohybrid was

employed as the modified material to fabricate an electrochemical sensor for the detection of kanamycin. The assay showed sensitive response to kanamycin in both buffer, milk and fish meal samples, indicating that the proposed method have great potential for analytical measurements in food safety.

2. Experimental

2.1 Reagents and materials

Zirconium (IV) chloride ($ZrCl_4$), N, N-Dimethylformamide (DMF) and 2-amino-1,4-benzenedicarboxylic acid (H_2N-BDC) were purchased from Sigma-Aldrich Co., Ltd (St Louis, MO, USA). Melamine, cyanuric acid, dimethyl sulfoxide and acetic acid were purchased from Aladdin Chemicals Co. Ltd. (Shanghai, China), Bovine serum albumin (BSA) was obtained from Sigma Aldrich (St. Louis, MO, USA). Other reagents were purchased from Chongqing Chuan-dong Chemical Co. Ltd. Deionized (DI) water was produced using a Milli-Q system. All chemicals were of analytical grade. All DNA oligonucleotides were purchased from Shanghai Sangon Biological Engineering Technology & Services Co., Ltd (Shanghai, China) and purified using high performance liquid chromatography, and the sequences of DNA oligonucleotides are given below: Kana aptamer (Apt): 5'-NH_2-$(CH_2)_6$ -TCTGGGGGTTGAGGCTAAGCCGACAG-3'; Complementary DNA of kana aptamer (cDNA): 5'-NH_2-$(CH_2)_6$-CTGTCGGCTTAGCCTCAACCCCCAGA-3'.

2.2 Instrumentations

All electrochemical measurements were performed on a CHI660D electrochemical

View Article Online
DOI: 10.1039/D0AY01503B

workstation (Shanghai CH Instruments Co. China) with a three-electrode system composed of platinum wire as auxiliary and Ag/AgCl electrode as reference. Cyclic voltammetry (CV) measurements were used to monitor the interface properties of the modified electrode. Square wave voltammetry (SWV) measurement was used to all detection of electrochemical performance of target kana. The morphologies of the nanocomposites were recorded on a Nova 400 scanning electron microscope (FEI, American). X-ray diffraction (XRD) pattern was operated on Bruker AXS D5005 (Bruker, Germany). X-ray photoelectron spectroscopy (XPS) measurements were conducted using a 5300 ESCA instrument (Perkin-Elmer PHI Co., USA). Fourier transformation infrared (FT-IR) spectra were recorded using a FT-IR spectrometer from Thermo Electron Co. (Nicolet 5700, USA).

2.3 Synthesis of UiO-66-NH_2, MCA, MWCNT@rGONR and UiO-66-NH_2/MCA/ MWCNT@rGONR nanocomposite

UiO-66-NH_2 was synthesized by the hydrothermal method [4]. The synthesis process was as follows: firstly, 73.43 mg $ZrCl_4$, 57.05 mg H_2BDC-NH_2 and 8.4 mL acetic acid were mixed in 70 mL DMF solution, and a homogeneous solution was formed by bath sonication. Next, the mixture was sealed in a Teflon-lined autoclave and heated in an oven at 120 °C for 24 hours. Before vacuum freeze-drying for 24 h, the buff products of UiO-66-NH_2 nanoparticles were collected by centrifuging (8,000 rpm, 8 min) and washed three times with methanol/DMF solution (v/v= 1:2).

MCA was synthesized of by the reported method [2]. First, equal molar amounts of cyanuric acid (0.51 g) and melamine (0.50 g) were dissolved in 20 and 10 mL dimethyl sulfoxide to form a homogeneous solution by vigorous stirring for 30 min. The white

precipitate was washed three times with ethanol, and then dried in an oven at 60 °C to obtain MCA supramolecular aggregates.

The synthesis of MWCNT@GONR was referred to the previous method with minor modifications [3]. In brief, 100 mg MWCNT was dispersed in 24 mL of concentrated H_2SO_4 (ω: 98%) and stirred at room temperature for 1 hour. Added 3 mL of H_3PO_4 (ω: 85%) to the system and stirred for 15 min. Then 300 mg of $KMnO_4$ was added and heated at 65°c for continuous stirring for 1.5 h before pouring into 133 ml of ice water containing H_2O_2 (4 ml, 30% vol) to terminate the reaction. MWCNT@rGONR with core-shell structure was prepared by the solution stripping method. The preparation steps are as follows: 2 mg mL^{-1} of MWCNT@GONR was sealed in a teflon-lined autoclave and heated at 180°C for 12 h. Before vacuum freeze-drying for 12 h, the products were collected by centrifuging (10000 rpm, 5min) and washed with deionized water and alcohol three times respectively.

6mg of amine-functionalized UiO-66-NH_2 was activated under gentle rotation at room temperature by 1 mL of 2.5% glutaraldehyde solution for 3h in PBS (pH=7.3). After centrifugation at 12,000 rpm, the nanoparticles were washed three times with 2 mL of PBS (pH=7.3). 3 mg of MCA, 6mg of MWCNT@rGONR and 1.5 mL DMF were added in the preparation system of UiO-66-NH_2 and stirred for 1h at room temperature.

2.4 Preparation of the UiO-66-NH_2/MCA/MWCNT@rGONR/GCE

First, the bare glassy carbon electrode (GCE) was polished to a mirror-like surface with 0.3 and 0.05 mM alumina slurry. Then washing ultrasonically with ultrapure water and absolute alcohol for three times, and dried with nitrogen. Dropped 5 μl of UiO-66-NH_2/MCA/

View Article Online
DOI: 10.1039/D0AY01503B

MWCNT@rGONR nanocomposite solution on the surface of the polished GCE and dried with nitrogen.

2.5 Fabrication of the aptasensor

Firstly, 5μL of cDNA (2.5μM) was dropped on the UiO-66-NH_2/MCA/ MWCNT@rGONR modified electrode and incubated at 35°C for 4 h and washed with Tris-HCl (10 mm, pH=7.2) solution and dried at room temperature. Secondly, to avoid nonspecific adsorption, 5μL of 0.025% BSA was added and incubated for 2 h to block the remaining active sites. Thirdly, 5μL of Apt (2.5μM) was dropped on the UiO-66-NH_2/MCA/MWCNT@rGONR/cDNA/BSA modified electrode and incubated at 35°C for 270 min and washed with Tris-HCl (10 mm, pH=7.2) solution and dried at room temperature. Fourthly, modified electrodes were immersed in methylene blue (MB) solution (25 μM) 30min, which was prepared with 0.1 M PBS. Finally, these electrodes were washed with Tris-HCl (10 mm, pH=7.2) solution three times and dried at room temperature. The resulting UiO-66-NH_2/MCA/MWCNT@rGONR/cDNA/BSA/Apt/MB modified electrodes were stored at 4 °C until use.

2.6 Electrochemical measurements

All electrochemical measurements including square wave voltammetry (SWV) and cyclic voltammetry(CV) were performed at room temperature using a three-electrode system consisting of a Ag/AgCl reference electrode, a platinum wire as the auxiliary electrode, and modified glassy carbon electrode (GCE) as the working electrode.

The electrochemical response was operated by SWV in 0.01M phosphate buffer saline (PBS) buffer (pH=7.2) on a CHI660D electrochemical workstation. SWV was recorded

within the potential range from -0.5 to 0 V at a pulse amplitude of 0.05 V and a pulse width scan of 0.06s. CV was performed within pH=7.2 PBS containing 1.0 mM $[Fe(CN)_6]^{3-/4-}$ (0.1M KCl) at a scan rate of 50 $mV \cdot s^{-1}$ and a scan potential of -0.2V ~ 0.6 V.

3 Result and discussion

3.1 Assembling of a nanohybrid aptasensor for kanamycin detection

As shown in Fig. 1, the preparation of nano-hybrid and the detection method of kanamycin were presented. Firstly, glutaraldehyde was used as an amino cross-linking agent to incubate the aptamer's complementary DNA (cDNA) on the electrode surface nano-hybrid materials (UiO-66-NH_2/MCA/MWCNT@rGONR). Next, after incubating BSA to block non-specific sites, the aptamer was fixed on the electrode surface by base complementary pairing with cDNA. Then, the methylene blue (MB) was used as an intercalator which can be inserted into double-stranded DNA (dsDNA) structure and produced a redox signal. Finally, when kanamycin specifically binds to the aptamer, the MB which inserted in the DNA double-strand was released, thereby resulting in a decrease on the peak current. We can obtain the kanamycin concentration according to the change of the peak current.

3.2 Characterization of the nanomaterials

The morphologies of the UiO-66-NH_2, MCA, MWCNT@rGONR, and UiO-66-NH_2/MCA/MWCNT@rGONR composite materials were examined using scanning electron microscopy (SEM), respectively (Fig. 2). The SEM image of UiO-66-NH_2 in Fig. 2a revealed that UiO-66-NH_2 had a distinct octahedral structure. The SEM image of MCA in Fig. 2b illustrated sphere-like structures, which was aggregated by multi-layered nanosheets

View Article Online
DOI: 10.1039/D0AY01503B

with many pores. In Fig. 2c, we can see the SEM image of MWCNT@rGONR. It can be clearly observed that MWCNT was covered by rGONR, while the center still maintains a tubular structure, which can prove the successful synthesis of MWCNT@rGONR core-shell structure nanomaterials. The SEM image of the UiO-66-NH_2/MCA/MWCNT@rGONR composite materials presented in Fig. 2d revealed that with MWCNT@rGONR as the substrate of the sensor interface material, UiO-66-NH_2 and MCA were evenly dispersed.

Fig. 3 presented the chemical element composition of UiO-66-NH_2 and UiO-66-NH_2/MCA/MWCNT@rGONR analyzed by the XPS. For UiO-66-NH_2, as shown in Fig. 3a, the C 1s XPS spectrum revealed three peaks with binding energies 288.5 eV (O–C=O), 283.9 eV (C–N), and 283.5 eV (C–C). The O 1s core-level XPS spectrum in Fig. 3b revealed four peaks at 530.4, 531.2, 531.7 and 532.7 eV, corresponding to the Zr-O, C-O, C=O and adsorbed oxygen to the surface of UiO-66-NH_2 [35], respectively. As presented in Fig. 3c, the Zr 3d peak can be decomposed into four peaks. The specific peaks at 182.2 eV and 184.5 eV correspond to the Zr-O bonds, the peaks at 182.8 eV and 185.0 eV correspond to the Zr-Zr bonds [35]. As shown in Fig. 3d, the N 1s core-level XPS spectrum revealed two peaks with binding energies 398.7 eV (N–H) and 400.1 eV (C–N).

On the other hand, for UiO-66-NH_2/MCA/MWCNT@rGONR, the XPS spectrum had some changes. As presented in Fig. 3e, compared with Fig.3a, the new high BEs at 287.5, 288.0 eV and 288.4eV are assigned with N=C-N, N-C=O and π-π *, respectively, which were originated from carbon at the spatial locations in the basic aromatic CN heterocycles and C 1s spectrum of MCA supramolecular aggregates [36]. The coexistence of N-C=O and N=C-N indicates UiO-66-NH_2/MCA was formed via Schiff-base condensation at a solid-vapor

interface [36]. It is not only favorable for improving the aptamer strands anchoring but also can enhance the electrochemical signal [37,38]. The O 1s core-level XPS spectrum in Fig. 3f, corresponding to the Zr-O to the surface of UiO-66-NH_2/MCA/MWCNT@rGONR at 529.6 eV. As presented in Fig. 3g, the Zr 3d peak can be decomposed into four peaks and the number of peaks did not change from Fig. 3c. As presented in Fig. 3h, the N 1s core-level XPS spectrum of UiO-66-NH_2/MCA/ MWCNT@rGONR was decomposed into three peaks at 398.2, 398.9 and 399.8 eV, which were ascribed to pyridinic N, pyrrolic N and graphitic N from the triazine configuration [39].

The successful synthesis of UiO-66-NH_2 was further confirmed by X-ray diffraction (XRD) pattern. As shown in Fig. S1, both UiO-66-NH_2 and UiO-66-NH_2/MCA/ MWCNT@rGONR showed the sharp characteristic peaks at $2\theta \approx 7.4°$ and 8.5°, which confirmed that UiO-66-NH_2 octahedra were successfully synthesized [40]. Fig. 4b showed that the main peaks for UiO-66-NH_2/MCA/MWCNT@rGONR retained no shift, demonstrating no change of the phase for UiO-66-NH_2 [35].

The above results demonstrated that the UiO-66-NH_2/MCA/MWCNT@rGONR composite was successfully prepared, thus they could provide abundant amino groups for the immobilization of aptamers.

3.3 Electrochemical characterization of the aptasensor

As shown in Fig. 4, cyclic voltammetric (CV) were recorded each step of the aptasensor manufacturing process with the scan rate of 100 mV/s. The oxidation-reduction reaction on the probe ($[Fe(CN)_6]^{4-/3-}$), the CV of the bare GCE showed a pair of distinct redox peaks (curve a). As shown in Fig. 4, the increased of the peak current in

UiO-66-NH_2/MCA/MWCNT@rGONR/GCE (curve c) was greater than UiO-66-NH_2/MCA/GCE (curve b), which confirmed that the charge transfer characteristics of MWCNT@rGONR was better than that of UiO-66-NH_2 or MCA. Because the insulating layer produced by the oligonucleotide interferes with electron transmission, the immobilized cDNA on the electrode surface significantly reduced the redox peak current (curve d). Since BSA blocks the remaining active sites, the addition of BSA resulted in a further reduction in current (curve e). The formation of the cDNA-Apt complex could hinder the transfer of electrons at electrode interface so that the current signal further decreased (curve f). Since the combination of cDNA and aptamer more tightly connected, making the three-level structures of them more firmly combined, allowing MB to attach to the DNA double-stranded structure. We explored the impact of using different sensor materials on detection. The electroactive surface area of different modified electrodes was calculated on the basis of the Randled−Sevcik equation.

$$I_p = 2.69 \times 10^5 n^{\frac{3}{2}} A D^{\frac{1}{2}} \nu^{\frac{1}{2}} C$$

Where Ip is the peak current (A); n is the number of transition electrons of $[Fe(CN)6]^{3-/4-}$(n=1); A refers to the effective surface area of the electrode (cm^2); D means the diffusion coefficient, ν means the scan rate (V/s), and C is the concentration of the redox reactant.

As a result, the electroactive effective surface area of different modified electrodes was calculated in the tendency of bare GCE < UiO-66-NH_2/MCA/GCE < UiO-66-NH_2/MCA/MWCNT@rGONR/GCE.

3.4 Optimization the performance of aptasensor

In order to achieve a satisfactory detection performance, the effect of several factors was investigated and optimized, including the MWCNT@rGONR concentration, cDNA concentration, incubation time of cDNA, kana reaction time, kana reaction temperature and capacity of composite.

In order to get the best performance of biosensor, the concentration of MWCNT@rGONR was evaluated. We verified in the pre-experiment that the MCA concentration had little effect on the signal response of the biosensor. Therefore, the concentrations of MCA and UiO-66-NH_2 remain unchanged. As shown in Fig. 5a, the current signal was changed with a concentration of MWCNT@rGONR, and reached maximized when the concentration was 2.0 mg mL^{-1}. Thus, 2.0 mg mL^{-1} was selected for the optimal concentration of MWCNT@rGONR.

It is important for the cDNA concentration incubation on the electrode surface to achieve maximized current signal. As shown in Fig. 5b, the peak current difference (ΔI) increased with the increase of cDNA concentration, which was reached maximized when the concentration was 2.5 μM. Therefore, the cDNA used in this work was 2.5 μM. The concentration of Apt was also selected at 2.5 μM depending on the pairing between oligonucleotides.

The immobilization time of cDNA was also showed in Fig. 5c. The ΔI increased rapidly with increasing immobilization time of cDNA to 270 min, because more cDNA were attached on the electrode. Then the ΔI growth was stable because the immobilization number of cDNA reached saturation. Therefore, an optimized immobilization time of 270 min was applied in this work.

View Article Online
DOI: 10.1039/D0AY01503B

In order to obtain a higher current response, the reaction time of the detection system was also optimized. As shown in Fig. 5d, the SWV signals reached equilibrium when the time was 35 min, because the construction of the Apt-kana complex on the electrode surface reached saturation. Therefore, 35 min was applied as the reaction time in this work.

As shown in Fig. 5e, it was observed that the current signal increased with the increase of reaction temperature and reached the maximum when the temperature was 35 °C. Thus, 35 °C was chosen as the reaction temperature in this work.

The load of composite materials was optimized. As shown in Fig. 5f, the peak current difference (ΔI) changed with the load of composite materials, which was reached maximized when the capacity was 5 μL. Therefore, the load of composite materials used in this work was 5 μL.

3.5 Calibration curve of aptasensor

Based on the above optimized conditions, a series of kana standard solutions with different concentrations were studied by SWV to investigate the analytical capabilities of the aptasensor. As shown in Fig. 6, the peak currents changed increased linearly with the concentration of kana in the range from 25 nM to 900 nM (0, 25, 50, 100, 150, 250, 350, 450, 600, 900 nM), the linear analysis of kana generated the following equation: y = 0.14+53.84x, and a correlation coefficient of 0.9991. The detection limit was determined to be 13 nM (S/N=3).

As compared with the reported aptasensors (Table 1), UiO-66-NH_2/MCA/ MWCNT@rGONR based ones have considerable detection range and detection performances. Compared with the platform materials of routine kana aptasensors, the

UiO-66-NH_2/MCA/ MWCNT@rGONR hybrid displayed three outstanding advantages, mainly including the following points: (i) UiO-66-NH_2, MCA and MWCNT@rGONR have good biocompatibility. Strong interaction between the cDNA and the UiO-66-NH_2/MCA, such as π-π stacking, electrostatic and hydrogen-bonding interactions, can enhance the cDNA immobilization and hybridization with kana aptamer. (ii) The instinct cavities inside the MOF and COF frameworks can not only promote aptamer strands to immobilize over the polyamino and porous structures but also can facilitate them to penetration into the pore channels further increased the number of aptamer strands binding and improved the detection performance. (iii) MWCNT@rGONR combined highly conjugated structure of MCA and the great biocompatibility of UiO-66-NH_2, which can enhance the conductivity and amplify electrochemical signal. Furthermore, the construction cost of the non-noble metal and non-enzyme nanomaterial hybrid system for our proposed sensor is much lower than it of the sensor in the literatures with the Au electrodes, gold nanoparticles and horseradish peroxidase.

3.6 The selectivity, stability and repeatability of the aptasensor.

In order to confirm the reliability of the constructed aptasensor, the binding selectivity of the aptasensor for 0.45 μM kana and other structural analogs (50 μM), such as streptomycin, furacilin, oxytetracycline, chlortetracycline, PBS (0.01 M) and some metal ions (80 μM) were evaluated. It can be seen in Fig. 7a, it was observed that the current induced by the addition of interfering substances were significantly different from kana. The results indicated the aptasensor had high specificity. The aptasensor was stored at 4 °C to estimate the stability of the aptasensor. The average response current of the five aptasensors against kana solution

decreased 7.42% after four 20 days of storage. The results indicated that the aptasensor had excellent stability, which can be seen from Fig. 7b. The excellent stability of the aptasensor could be attributed to the performance of the electrode base materials and the stability anchoring of the aptamers. In order to investigate the repeatability of the fabricated aptasensor, a fresh batch of five aptasensors were prepared and used to detect the mixture of kana. As shown in Fig. 7c, the relative standard deviations (RSDs) of the measurements was 2.61% for kana (n=3), which indicated that the constructed electrochemical aptasensor was sensitive and applicable.

3.7 Analysis of kana in fish meat and milk

For studying the feasibility and accuracy of the constructed aptasensor, it was used to detect the recoveries of different concentrations of kanamycin in animal-derived food by the above standard methods. Fish meat and milk samples were obtained from a local market. Subsequently, to avoid unspecific adsorption of fish meat and milk, we diluted the spiked samples 100-fold. Samples with different kanamycin spiked concentrations of 0.1, 0.15, 0.25, 0.5 and 0.6 μM were analyzed by the proposed aptasensor. As shown in Table 2, the average recoveries were obtained within the range of 98.3~107.7% for fish meat and 97.8~103.7% for milk and the RSD was in the range from 2.01% to 4.86% respectively. Thus, the constructed aptasensor can be effectively applied to the quantitative detection of kanamycin in animal-derived foods.

4. Conclusion

In summary, a selective electrochemical method was investigated for kana detection

based on the specific interactions between aptamers, UiO-66-NH_2/MCA and MWCNT@rGONR. Due to the specific recognition of space sites by DNA aptamer and the characteristics of electrode materials leading to the amplification of electrical signals, this method shows high detection selectivity, stability and sensitivity. This biosensor was also proved to possess the applicability for detecting kana in milk and fish meal samples. More importantly, if the aptamer was replaced by other antibiotic's aptamer, this method can also be used to detect other antibiotics proving that this sensor has good application prospects. Using this method, kanamycin was easily detected at level as low as 13 nM within linearity of the kana concentration of 25~900 nM, which is far below the MRL (62 nM in Korea, 206 nM in the European Union, and 83 nM in Japan) in food products. Although this method has the shortcoming of the relatively time-consuming step by step assembling, it still has the characteristics of simple operation, inexpensive instrument, cheap instrument, low cost and high selectivity, which make it attractive method for antibiotic detection. Compared with the platform materials of routine kana aptasensor, the UiO-66-NH_2/MCA/MWCNT@rGONR hybrid displays some outstanding advantages. This work can provide a new idea and method for the construction of electrochemical sensors, and broaden its application in the fields of food safety and bio-sensing.

Acknowledgment

This work was supported by National Natural Science Foundation of China (No. 81271930 and 31000425), the Research Project of Chongqing Science and Technology Commission of China (cstc2020jcyj-msxmX0861), the Fundamental Research Funds for the Central

View Article Online
DOI: 10.1039/D0AY01503B

Universities (2020CDJ-LHZZ-033), and we would like to thank Analytical and Testing Center of Chongqing University for SEM images, XRD and FT-IR spectrum.

References

1. David and Stead, *Journal of Chromatography B Biomedical Sciences & Applications*, 2000.
2. G. Al-Malky, S. J. Dawson, T. Sirimanna, E. Bagkeris and R. Suri, *Journal of Cystic Fibrosis*, 2015, **14**, 248-254.
3. G. M. Pacifici, *MedicalExpress*, 2015, **2**, M150501-M150501.
4. L. P. Kotra, J. Haddad and S. Mobashery, *Antimicrobial Agents and Chemotherapy*, 2000, **44**, 3249-3256.
5. H. W. Taber, J. P. Mueller, P. F. Miller and A. S. Arrow, *Microbiological Reviews*, 1987, **51**, 439-457.
6. M. Pendela, J. Hoogmartens, A. Van Schepdael and E. Adams, *Journal of Separation Science*, 2009, **32**, 3418-3424.
7. I. Prokhorova, R. B. Altman, M. Djumagulov, J. P. Shrestha, A. Urzhumtsev, A. Ferguson, C.-W. T. Chang, M. Yusupov, S. C. Blanchard and G. Yusupova, *Proceedings of the National Academy of Sciences of the United States of America*, 2017, **114**, E10899-E10908.
8. A. A. Rowe, E. A. Miller and K. W. Plaxco, *Analytical Chemistry*, 2010, **82**, 7090-7095.
9. R. H. M. M. Granja, A. M. Montes Nino, R. A. M. Zucchetti, R. E. Montes Nino, R. Patel and A. G. Salerno, *Analytica Chimica Acta*, 2009, **637**, 64-67.
10. P. Vinas, N. Balsalobre and M. Hernandez-Cordoba, *Talanta*, 2007, **72**, 808-812.
11. P. Edder, A. Cominoli and C. Corvi, *Journal of Chromatography A*, 1999, **830**, 345-351.
12. J. Wang, D. Wang, K. Ni and X. Hu, *Journal of Liquid Chromatography & Related Technologies*, 2007, **30**, 1001-1013.
13. K. R. Copeland and R. W. Yatscoff, *Therapeutic Drug Monitoring*, 1988, **10**, 453-458.
14. S. Niu, Z. Lv, J. Liu, W. Bai, S. Yang and A. Chen, *Plos One*, 2014, **9**.
15. Y. Xu, T. Han, X. Li, L. Sun, Y. Zhang and Y. Zhang, *Analytica Chimica Acta*, 2015, **891**, 298-303.
16. N.-R. Ha, I.-P. Jung, S.-H. Kim, A. R. Kim and M.-Y. Yoon, *Process Biochemistry*, 2017, **62**, 161-168.
17. E. Usleber, M. Lorber, M. Straka, G. Terplan and E. Martlbauer, *Analyst*, 1994, **119**, 2765-2768.
18. L. Hao, H. Gu, N. Duan, S. Wu and Z. Wang, *Analytical Methods*, 2016, **8**, 7929-7936.
19. M. Zhao, Y. Zhuo, Y.-Q. Chai and R. Yuan, *Biomaterials*, 2015, **52**, 476-483.
20. H. Kubo, Y. S. Huang and T. Kinoshita, *Bunseki Kagaku*, 1989, **38**, 215-217.
21. Z. L. Zhi, U. J. Meyer, J. W. Van den Bedem and M. Meusel, *Analytica Chimica Acta*, 2001, **442**, 207-219.
22. Y. Xin, Z. Li and Z. Zhang, *Chemical Communications*, 2015, **51**, 15498-15501.
23. L. S. Khabbaz, M. Hassanzadeh-Khayyat, P. Zaree, M. Ramezani, K. Abnous and S. M. Taghdisi, *Analytical Methods*, 2015, **7**, 8611-8616.

24. C. Liu, C. Lu, Z. Tang, X. Chen, G. Wang and F. Sun, *Microchimica Acta*, 2015, **182**, 2567-2575.
25. M. Ramezani, N. M. Danesh, P. Lavaee, K. Abnous and S. M. Taghdisi, *Sensors and Actuators B-Chemical*, 2016, **222**, 1-7.
26. B. Zhou, B. Shi, D. Jin and X. Liu, *Nature Nanotechnology*, 2015, **10**, 924-936.
27. W. Guo, N. Sun, X. Qin, M. Pei and L. Wang, *Biosensors & Bioelectronics*, 2015, **74**, 691-697.
28. X. Qin, Y. Yin, H. Yu, W. Guo and M. Pei, *Biosensors & Bioelectronics*, 2016, **77**, 752-758.
29. M. Chen, N. Gan, Y. Zhou, T. Li, Q. Xu, Y. Cao and Y. Chen, *Talanta*, 2016, **161**, 867-874.
30. Y. Zhu, P. Chandra, K.-M. Song, C. Ban and Y.-B. Shim, *Biosensors & Bioelectronics*, 2012, **36**, 29-34.
31. N. Zhou, Y. Ma, B. Hu, L. He, S. Wang, Z. Zhang and S. Lu, *Biosensors & Bioelectronics*, 2019, **127**, 92-100.
32. M. Chen, N. Gan, Y. Zhou, T. Li, Q. Xu, Y. Cao and Y. Chen, *Sensors and Actuators B-Chemical*, 2017, **242**, 1201-1209.
33. T. Devic, C. Serre, N. Audebrand, J. Marrot and G. Ferey, *Journal of the American Chemical Society*, 2005, **127**, 12788-12789.
34. N. A. A. Qasem, R. Ben-Mansour and M. A. Habib, *Applied Energy*, 2018, **210**, 317-326.
35. X. He, F. Deng, T. Shen, L. Yang, D. Chen, J. Luo, X. Luo, X. Min and F. Wang, *Journal of Colloid and Interface Science*, 2019, **539**, 223-234.
36. Y. Guo, J. Li, Y. Yuan, L. Li, M. Zhang, C. Zhou and Z. Lin, *Angewandte Chemie-International Edition*, 2016, **55**, 14693-14697.
37. S. Bi, C. Lu, W. Zhang, F. Qiu and F. Zhang, *Journal of Energy Chemistry*, 2018, **27**, 99-116.
38. J. Zhao, B. J. Hansen, Y. Wang, T. A. Csepe, L. V. Sul, A. Tang, Y. Yuan, N. Li, A. Bratasz, K. A. Powell, A. Kilic, P. J. Mohler, P. M. L. Janssen, R. Weiss, O. P. Simonetti, J. D. Hummel and V. V. Fedorov, *Journal of the American Heart Association*, 2017, **6**.
39. C. Hu and L. Dai, *Advanced Materials*, 2017, **29**.
40. M. Liu, J. Wang, Q. Yang, N. Hu, W. Zhang, W. Zhu, R. Wang, Y. Suo and J. Wang, *Food Chemistry*, 2019, **270**, 1-9.
41. X. Bai, H. Hou, B. Zhang and J. Tang, *Biosensors & Bioelectronics*, **56**, 112 (2014).
42. Y. Wang, T. Ma, S. Ma, Y. Liu and J. Wang, *Microchimica Acta*, **184**, 1 (2017).
43. K. H. Leung, H. Z. He, S. H. Chan, W. C. Fu, C. H. Leung and D. L. Ma, *Sensors & Actuators B Chemical*, **B177**, 487 (2013).
44. Y. P. Xing, C. Liu, X. H. Zhou and H. C. Shi, *Scientific Reports*, **5**, 8125 (2015).
45. Yunfei, Tang, Chunmei, Gu, Cheng, Wang, Baodong, Song, Xiaohong and Zhou, *Biosensors & Bioelectronics: The International Journal for the Professional Involved with Research, Technology and Applications of Biosensers and Related Devices* (2018).
46. X. Sun, F. Li, G. Shen, J. Huang and X. Wang, *Analyst*, **139**, 299 (2014).
47. F. Li, Y. Guo, X. Sun and X. Wang, *European Food Research and Technology*, **239**, 227 (2014)
48. M. Liu, J. Wang, Q. Yang, N. Hu, W. Zhang, W. Zhu, R. Wang, Y. Suo and J. Wang, *Food Chemistry*, 2019, **270**, 1-9.

49. F. Li, Z. Yu, X. Han, W. Shi, Y. Liu, H. Yan and G. Zhang, *Sensors and Actuators B-Chemical*, 2018, **273**, 480-487.

50. F. Li, X. Wang, X. Sun and Y. Guo, *Rsc Advances*, 2017, **7**, 38981-38988.

View Article Online
DOI: 10.1039/D0AY01503B

Table 1 The proposed assay compared with other methods for the detection of kana.

Materials	Method	LOD(nM)	Linear range	Ref.
aptamer-based cantilever array	cantilever	5000	100 μM - 10 mM	[41]
MoS_2 nanosheets and carbon dots	fluorometric	1100	4 μM - 25 μM	[42]
oligonucleotide	fluorometric	143	0.2 μM - 150 μM	[43]
G-quadruplex DNA aptamer	electrochemiluminescent	59	0.1 μM - 20 μM	[44]
graphene oxide and DNA aptamer	fluorometric	26	200 nM - 200 μM	[45]
gold nanoparticles/multi-walled carbon nanotubes	electrochemistry	5.8	10 nM - 150 nM	[46]
gold nanoparticles/graphene–polyaniline composite film	electrochemistry	8.6	10 nM - 200 nM	[47]
Au electrode and methylene blue (MB)-labelled signaling probe	electrochemistry	0.0033	0.07 nM - 1.0 μM	[48]
double-stranded DNA (dsDNA) modified with cadmium sulfide (CdS) nanoparticles and gold nanoparticles	electrochemistry	9.76	10 nM - 450 nM	[49]
Gold nanoparticles (AuNPs) and HRP–AuNP–cDNA conjugates	electrochemistry	5	10 nM - 150000 nM	[50]
UiO-66-NH_2/MCA/MWCNT@rGONR	the present assay	13	25 nM - 900 nM	This work

View Article Online
DOI: 10.1039/D0AY01503B

Table 2 The detection of kana in milk and fish samples.

Real samples	Added(μM)	Found(μM)	Recovery(%)	RSD(%, n=3)
Milk	0.1	0.097	99.1	3.64
	0.15	0.155	97.8	2.58
	0.25	0.251	100.2	2.99
	0.5	0.49	103.7	2.75
	0.6	0.584	102.4	2.01
Fish meal	0.1	0.105	107.7	4.86
	0.15	0.145	101.9	2.35
	0.25	0.246	98.3	2.14
	0.5	0.518	103.8	2.76
	0.6	0.603	104.5	2.64

View Article Online
DOI: 10.1039/D0AY01503B

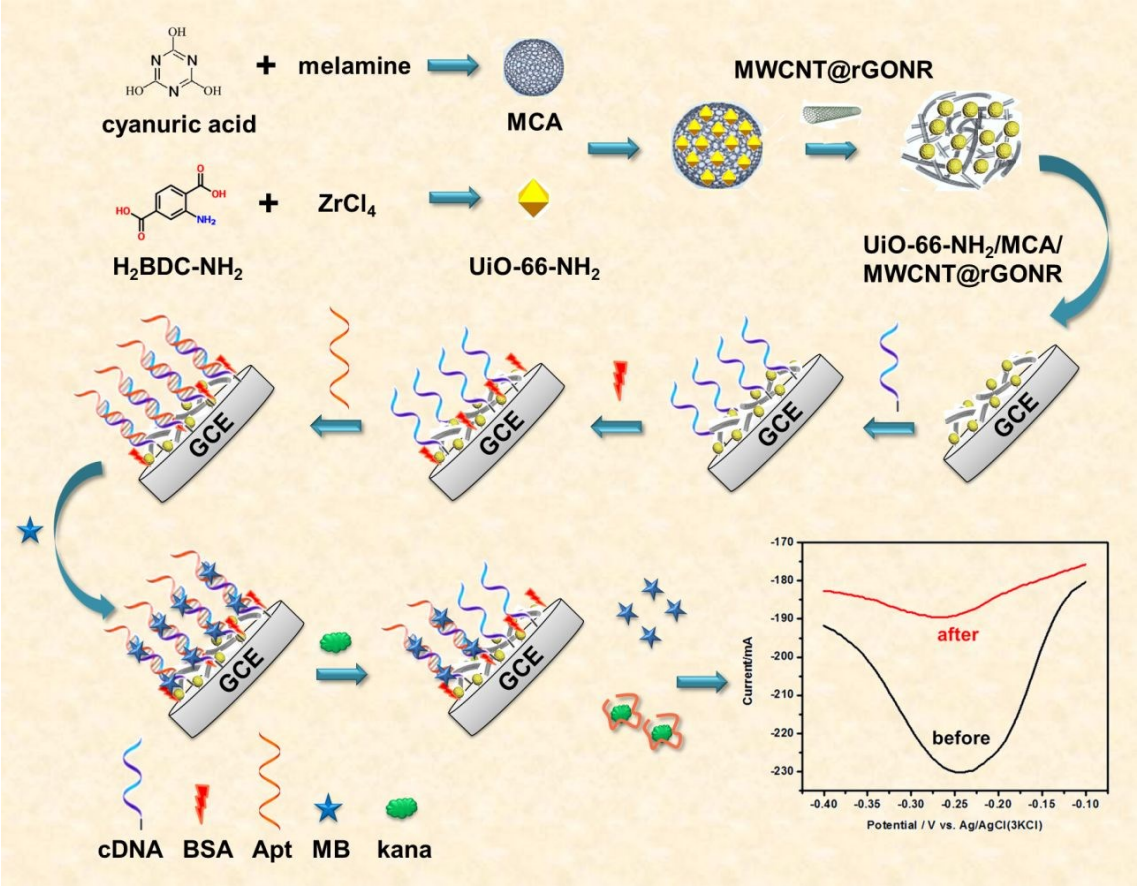

Fig. 1 Schematic illustration of the fabrication of the aptasensor.

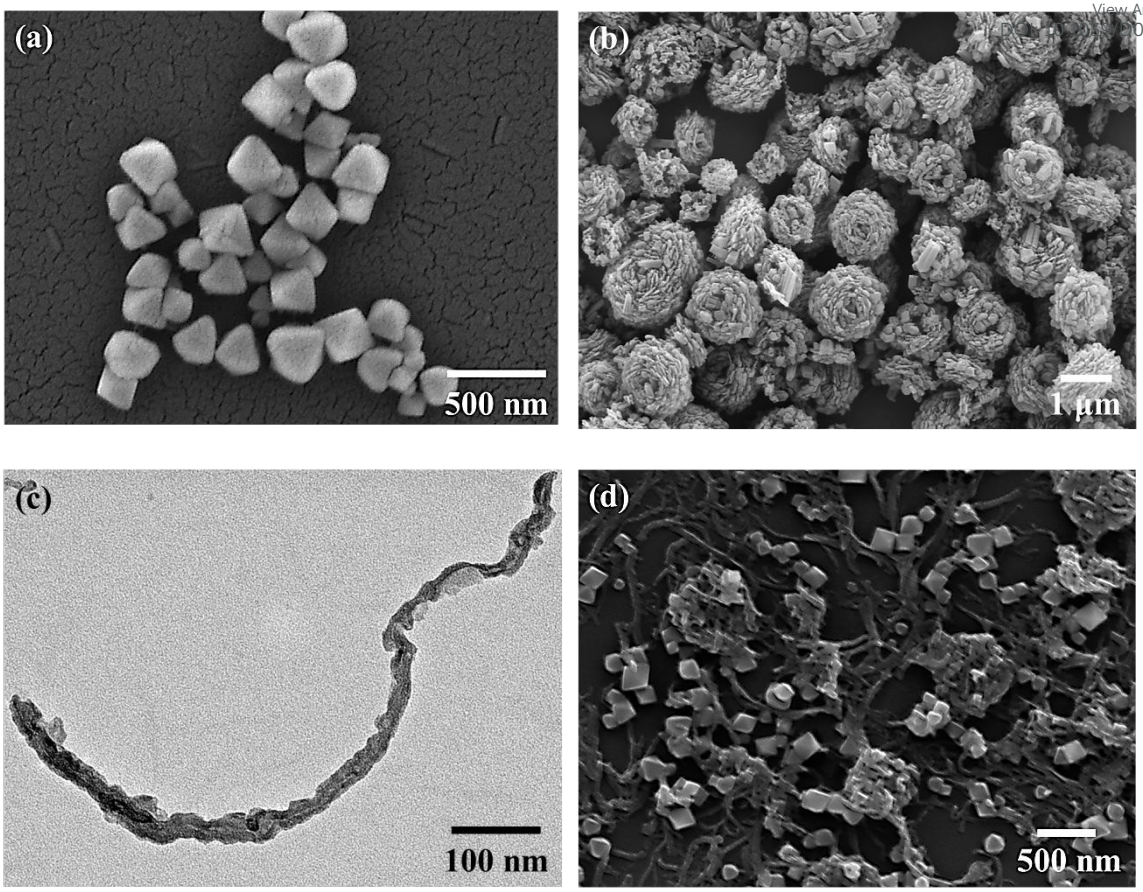

Fig. 2 SEM images of UiO-66-NH_2 (a), MCA (b), MWCNT@rGONR (c), UiO-66-NH_2/MCA/MWCNT@rGONR nanocomposite (d).

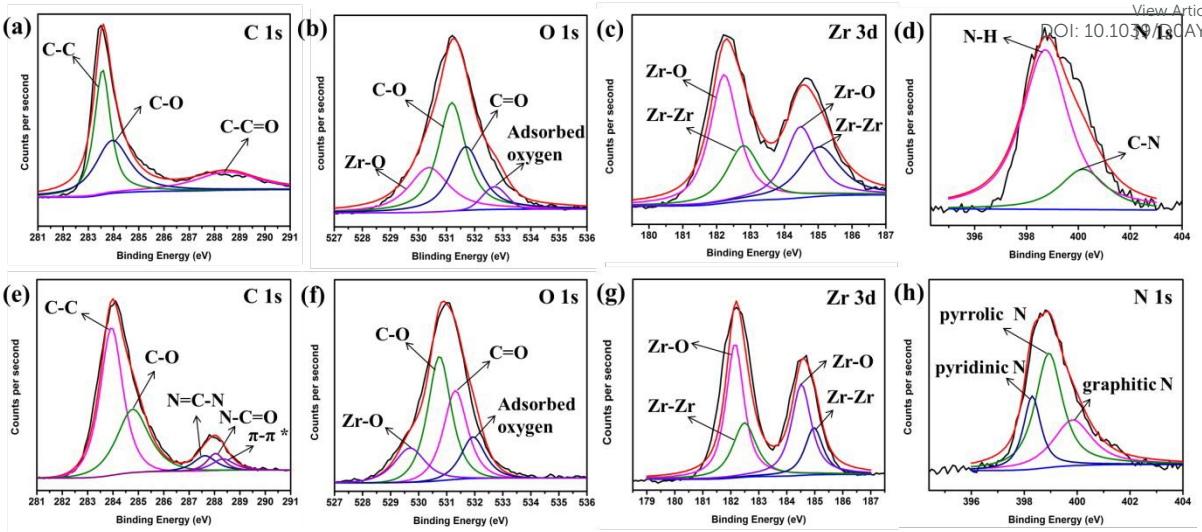

Fig. 3 C 1s, O 1s, Zr 3d and N 1s core-level XPS spectra of UiO-66-NH_2 (a, b, c, d) and UiO-66-NH_2/MCA/MWCNT@rGONR (e, f, g, h).

View Article Online
DOI: 10.1039/D0AY01503B

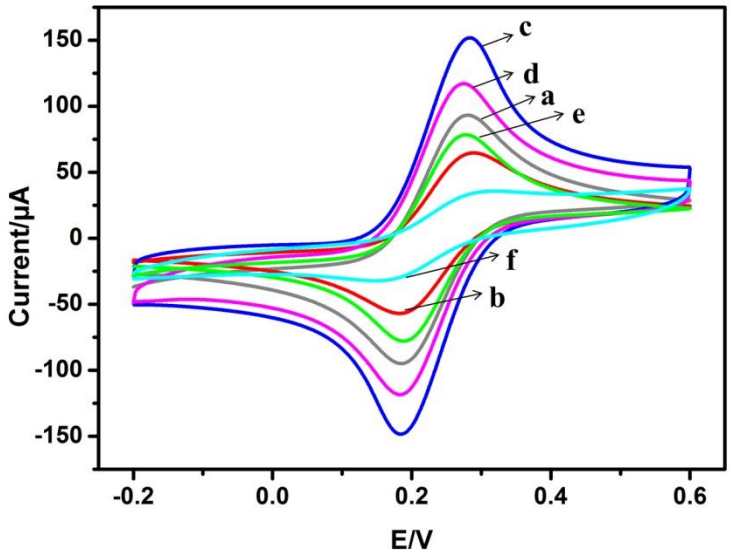

Fig. 4 CV obtained at the GCE (a), UiO-66-NH_2/MCA/GCE (b), UiO-66-NH_2/MCA/MWCNT@rGONR/GCE (c), UiO-66-NH_2/MCA/MWCNT@rGONR/cDNA/GCE (d), UiO-66-NH_2/MCA/MWCNT@rGONR/cDNA/BSA/GCE (e), UiO-66-NH_2/MCA /MWCNT@rGONR/cDNA/BSA/Apt/GCE (f) respectively. (in 1.0 mM $[Fe(CN)_6]^{3-/4-}$ solution containing 0.1 M KCl at a scan rate of 50 mV/s and a scan potential of -0.2 ~ 0.6 V)

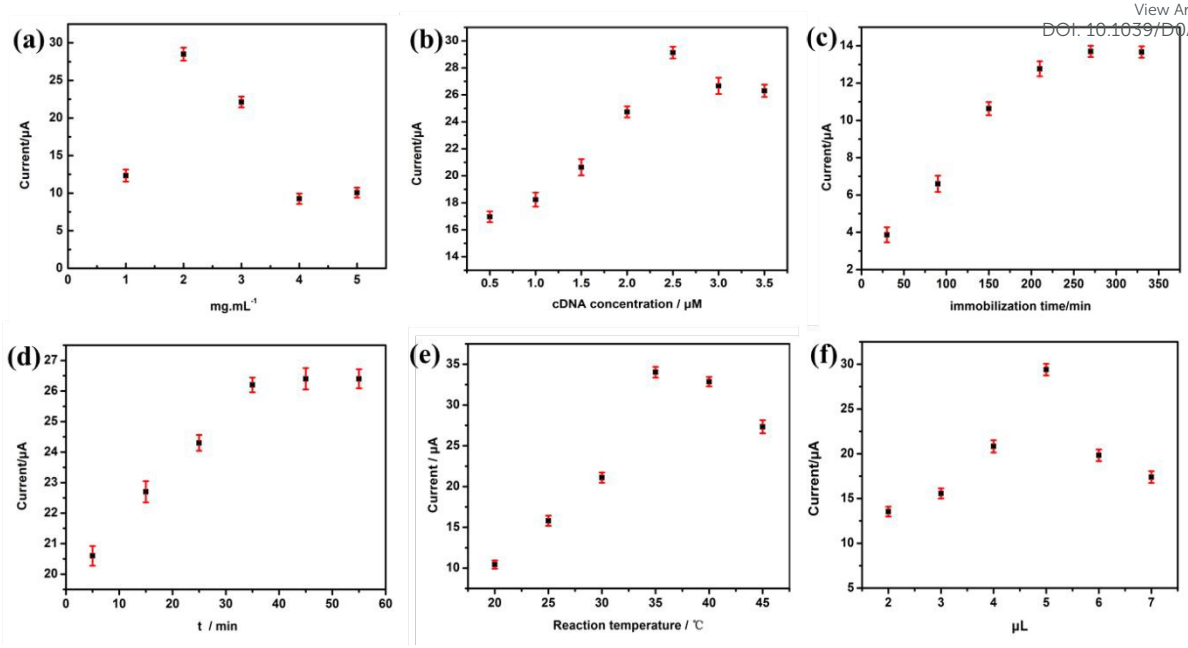

Fig. 5 Effect of concentration of MWCNT@rGONR (a), incubation concentration of cDNA (b), immobilization time of cDNA (c), reaction time of the detection system (d), reaction temperature (e), and the load of composite materials (f) on the SWV peak current.

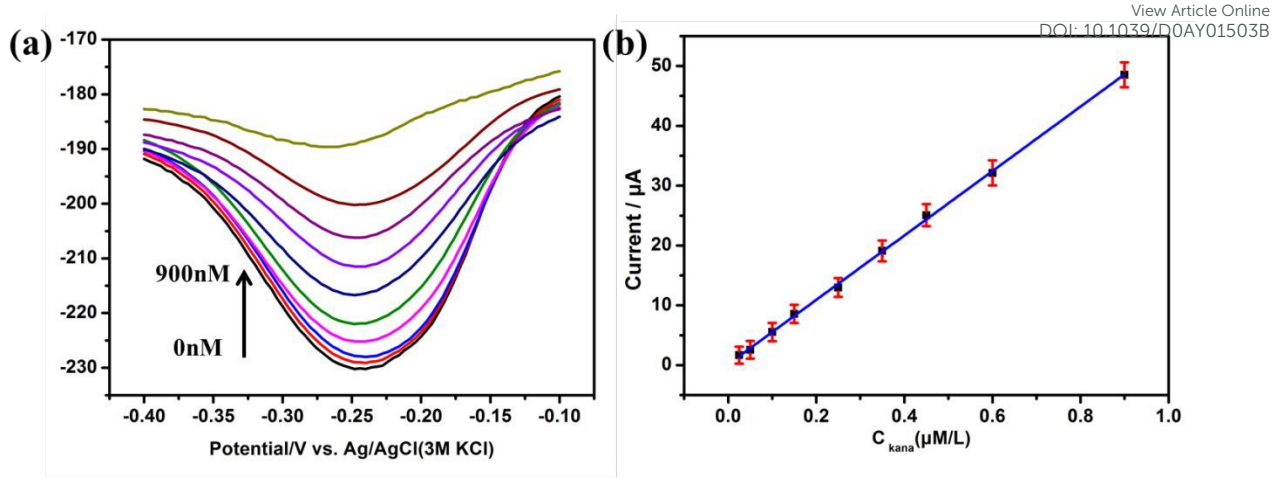

Fig. 6 SWV obtained for prepared aptasensor recorded in 0.1 M PBS (pH 7.2) after incubation with different concentration of kana in the range from 25 ~ 900 nM (0, 25, 50, 100, 150, 250, 350, 450, 600, 900 nM) (a); Linear diagram of peaks current and kana concentration (b).

View Article Online
DOI: 10.1039/D0AY01503B

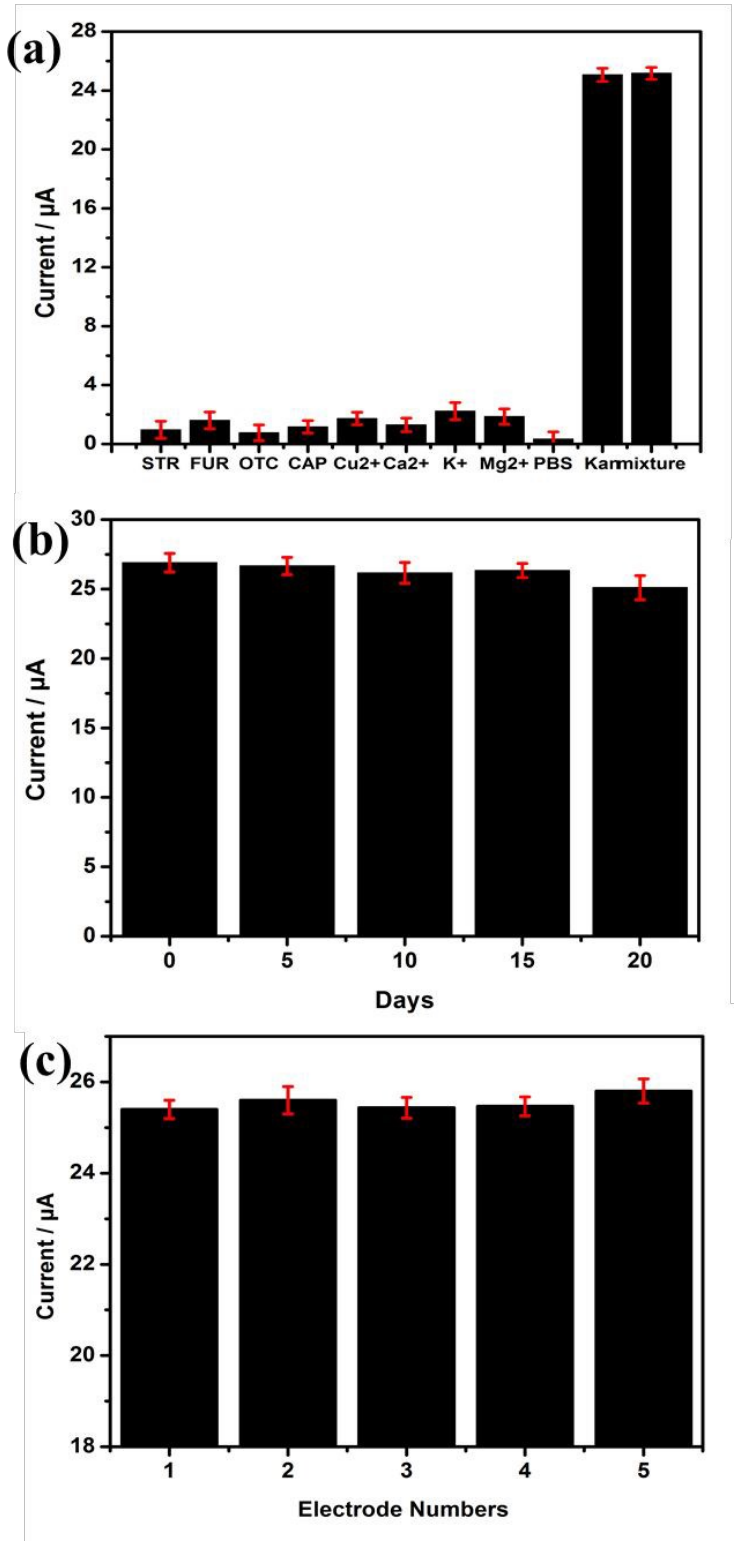

Fig. 7 The selectivity (a) of the aptasensor for detection of 0.45 μM kana with the interference of streptomycin (50 μM), furacilin (50 μM), oxytetracycline (50 μM), chlortetracycline (50 μM), PBS (0.01 M) and some metal ions (80 μM); the repeatability (b) and stability (c) of the aptasensor (n = 3).